J. Opt. A: Pure Appl. Opt. **9** (2007) S366–S371 doi:10.1088/1464-4258/9/9/S14

Comparison of finite-difference time-domain simulations and experiments on the optical properties of gold nanoparticle arrays on gold film

Andreas Hohenau[1], **Joachim R Krenn**[1], **Francisco J Garcia-Vidal**[2], **Sergio G Rodrigo**[3], **Luis Martin-Moreno**[3], **Jonas Beermann**[4] **and Sergey I Bozhevolnyi**[4]

[1] Karl-Franzens University and Erwin Schrödinger Institute for Nanoscale Research, A-8010 Graz, Austria
[2] Departamento de Fisica Teorica de la Materia Condensada, Universidad Autonoma de Madrid, E-28049 Madrid, Spain
[3] Departamento de Fisica de la Materia Condensada, ICMA-CSIC, Universidad de Zaragoza, E-50009 Zaragoza, Spain
[4] Department of Physics and Nanotechnology, Aalborg University, DK-9220 Aalborg Øst, Denmark

E-mail: andreas.hohenau@uni-graz.at

Received 31 January 2007, accepted for publication 1 March 2007
Published 23 August 2007
Online at stacks.iop.org/JOptA/9/S366

Abstract
We present experimental and simulated results of far-field reflection spectroscopy and two-photon luminescence microscopy of arrays of gold nanoparticles on gold film. These arrays are intended as a simplified model system compared to random arrangements of gold particles on gold film, which show huge surface enhancements for, e.g., Raman scattering of adsorbed molecules, related to the enhanced optical near-fields. By a detailed comparison of the experimental results to the finite-difference time-domain simulations (without free fitting parameters), we can identify the modes responsible for the enhancement in intensity on the investigated substrates. The qualitative and quantitative validity of the theoretical approach is addressed and we discuss the origin of the observed differences between theory and experiment as well as possible routes to overcome them.

Keywords: surface plasmons, FDTD, nanoparticles, particle array, grating coupling, two-photon luminescence, optical near-field

1. Introduction

Random arrangements of gold particles on gold film are well-known substrates for the observation of strong surface enhanced effects like surface enhanced Raman scattering (SERS) [1, 2], surface enhanced two-photon luminescence (TPL) [3, 4], or surface enhanced luminescence [5, 6]. The physical mechanism responsible for the surface enhanced effects is at least partly related to the strong optical near-fields close to resonantly driven surface plasmons on nano-structured metal (usually gold or silver) surfaces [7]. On random substrates (e.g. deposited colloid, electrochemically roughened or evaporated films) so-called 'hot-spots' are observed, i.e. strongly localized areas on the substrate, where the enhancement is particularly strong [1]. For these hot-spots, record enhancement values for SERS of up to 10^{14} have been reported [2]. These huge enhancements are considered to be related to narrow gaps between neighbouring nanoparticles, which are electromagnetically coupled across the narrow gap, thereby causing huge fields inside the gap [1].

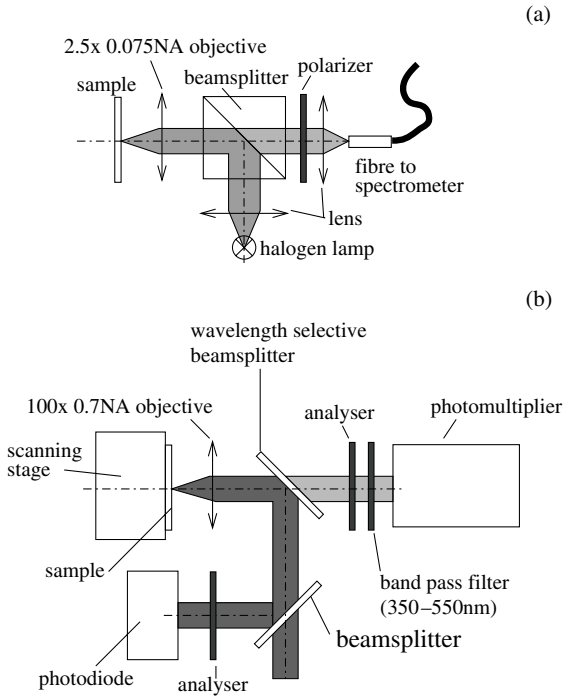

Figure 1. Experimental setups for (a) reflection spectroscopy, and (b) TPL microscopy.

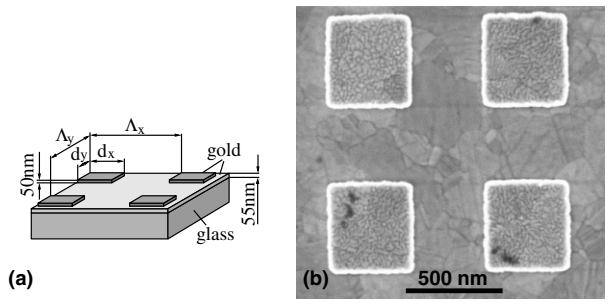

Figure 2. (a) Sketch of the sample's geometry, and (b) exemplary SEM image of the sample with $\Lambda_x = 760$, $\Lambda_y = 750$ nm and $d_x = d_y = 456$ nm.

This interpretation is qualitatively supported by different simulations, but a detailed understanding of the effect is still missing. On the one hand, numerical simulations are challenging due to computational limits causing restrictions to the minimal cell size and due to the limited knowledge of the (non)local behaviour of the metal dielectric function in these size regimes. On the other hand, these very narrow gaps are also experimentally demanding, both in the exact metrological characterization below the 10 nm range and the reproducible fabrication of such structures with nanometer precision or better.

Our aim in this paper is to gain a better understanding of the physics involved in the optical excitation of nanostructured metal surfaces as well as testing the applicability of finite-difference time-domain simulations (FDTD) based on macroscopic Maxwell equations to describe such systems. As a suitable substrate for these comparative investigations, we chose regular arrays of rectangular gold nanoparticles on a gold surface.

2. Experimental details

2.1. Characterization techniques

The characterization of the samples is performed experimentally using two methods: optical reflection spectroscopy (figure 1(a)) to access the far-field properties and two-photon induced luminescence (TPL) microscopy for characterization of the optical near-fields (in the wavelength range of 720–900 nm, figure 1(b)).

Reflection spectra are recorded by a Zeiss MMS-1 microspectrometer attached to a conventional optical microscope (figure 1(a)) equipped with a 2.5×, 0.075 numerical aperture (NA) objective. To control the polarization of the reflected light, a polarizer is inserted in the optical path of the microscope. The reference for the reflection spectra was taken on a plain, unstructured gold film outside the areas covered with particle arrays. The spectra therefore directly reflect the changes induced by the particle arrays, as compared to the plain film.

The experimental setup for TPL scanning microscopy is shown schematically in figure 1(b) and described in [8]. It allows us to record simultaneously the TPL signal (detected by a photomultiplier) and the backscattered light (detected by a photodiode) as a function of the sample position with a spatial resolution determined by the focal spot size of the excitation laser at the sample surface (∼1 μm) [9]. In this experiment, we use a 200 fs Ti:sapphire laser at a repetition rate of 80 MHz with a linewidth of ∼10 nm and an adjustable polarization plane. The laser wavelength can be tuned between 720 and 900 nm, which allows us to make spectrally resolved studies of TPL efficiency. The typical average incident power is in the range 0.1–50 mW.

2.2. Investigated samples

To allow for unambiguous comparison between experiments and model calculations despite the spectral restrictions of the TPL setup, the maximum field enhancements should appear in the spectral range of 720–900 nm and the arrays should have a defined and controllable geometry. In view of the unavoidable geometrical uncertainties of the fabricated samples and restrictions to the minimal cell size of space discretization in the model calculations, it is necessary to consider relatively simple geometries only, and avoid, for example, narrow gaps which, on the one hand, are expected to yield extremely high field enhancements that are important for TPL, but on the other hand depend critically on geometrical details which are not readily accessible by experimental methods (e.g. gap width, surface topography in the range below 1 nm, crystal orientation etc).

The investigated system therefore consists of regular gold nanoparticle arrays on top of a 55 nm thick gold film (figure 2), fabricated by electron beam lithography [10]. The relatively large lateral particle dimension (100–500 nm) and array periods (700–900 nm) assure that some nanometer variations in the different particle and array dimensions will not lead to strong variations in the optical properties of the arrays.

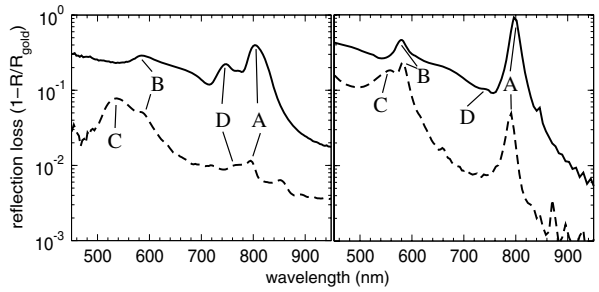

Figure 3. (a) Measured and (b) simulated reflection-loss spectra of the sample with $\Lambda_x = 760$ nm, $\Lambda_y = 750$ nm and $d_x = d_y = 465$ nm (solid lines) and the sample with $\Lambda_x = \Lambda_y = 780$ nm and $d_x = d_y = 150$ nm (dashed line). The particle height is 50 nm and the polarization is parallel to x.

Despite the large particle distances, the 55 nm thick gold film below the particles still ensures a considerable coupling between the individual particles, as they interact strongly through the excitation of surface plasmon polaritons (SPP) guided at the gold–air interface [11]. Generally, a metal film in an asymmetric environment (glass and air) supports two SPP modes: the s-mode with a field maximum at the gold–air interface, and the a-mode with a field maximum at the gold–glass interface. The chosen gold film thickness of 55 nm is sufficient to practically suppress the coupling of the particles to a-mode SPPs, thereby keeping the number of possible excitation channels at a minimum.

3. The optical resonances probed by reflection spectroscopy

3.1. Experimental results

To discuss the optical modes present in such arrays, we analyse the reflection spectra recorded at normal incidence with the micro-spectrometer setup. Typical reflection spectra (reference acquired on the plain gold film) are depicted in figure 3 for array dimensions of $\Lambda_x = 760$ nm, $\Lambda_y = 750$ nm and $d_x = d_y = 465$ nm (solid lines) and $\Lambda_x = \Lambda_y = 780$ nm and $d_x = d_y = 150$ nm (dashed line). The spectra are dominated by two bands, which can be assigned to grating coupling to SPP modes in the [1 0] (peak 'A') and [1 1] (peak 'B') grating order by comparing their spectral position for various array periods against the dispersion relation of SPP at the gold–air interface [12]. Additionally, for the smaller particles, a less prominent band at ∼520 nm (peak 'C') is observed, whose spectral position is basically independent of the array period [12], and which can therefore be attributed to a resonance localized to the individual particles (i.e. a localized surface plasmon (LSP) mode). However, it should be noted that, since our particles are relatively large and are sited directly on the gold film, we expect the particle's horizontal dipolar LSP resonance, as it would be seen on a gold nanoparticle in a dielectric environment, to be shifted beyond a wavelength of 1000 nm out of the spectral region accessible by our experimental setup [13] (this resonance could be tuned to overlap with one of the grating-coupling peaks by adding a dielectric spacer between the gold film and the particles [13, 14]). Also, in contrast to the LSP of gold nanoparticles in a dielectric environment, the resonance of peak 'C' is only weakly dependent on the particle shape and always stays close to ∼520 nm [12]. Finally, peak 'D' can be related to light modes scattered at a grazing angle at the gold–air interface (the Wood anomaly).

3.2. Comparison to simulations

For comparison, figure 3(b) depicts the results of FDTD simulations for infinite arrays with the same geometrical parameters as the experimentally investigated arrays. The details for the simulations can be found in [15], however for the following discussion it is important to note that the simulations do not contain any free fitting parameters, but are based on the geometry of the sample (as measured by scanning electron microscopy (SEM)) and the literature values for the dielectric function of gold of [16]. By comparing figures 3(a) and (b), a very good qualitative accord can be observed, although there are two obvious differences to the experimental spectra. First, the simulated spectra show more pronounced and spectrally narrower peaks. Second in the simulations, one peak at the short wavelength wing of the [1 0] SPP mode is so small that it can hardly be observed in figure 3(b).

4. Optical near-fields

Additionally to the far-field spectra, FDTD simulations allow us to compute the optical near-fields of the arrays. For example, for the sample with the largest particles, the images of the optical near-field intensity at the two SPP resonances (580 nm ([1 1] resonance) and 800 nm ([1 0] resonance)) are depicted in figure 4, in x–y planes 5 nm below and above the gold–air interface, and in the x–z planes through the centre of the particles. In the case of the excitation at the [1 1] resonance, four equivalent SPP modes are excited: [1 1], [1 −1], [−1 1] and [−1 −1], i.e. four SPP waves which propagate in the diagonal directions. On a flat interface the interference of these waves would lead to a characteristic interference pattern depicted in the inset of figure 4(a). In the case of excitation with light of wavelength 800 nm, only the [1 0] and [−1 0] SPP modes are excited, whose interference leads to a standing wave pattern with wavefronts parallel to the y-direction, which in the case of a flat interface would lead to the pattern depicted in the inset of figure 4(b). Here, qualitatively similar patterns are observed, but there are also geometrically induced strongly localized near-fields at the particle edges, which contribute considerably to the overall near-field intensity and lead to a less obvious appearance of the characteristic [1 1] and [1 0] pattern (figures 4(a)–(d)). For smaller particles ($d_x = d_y \simeq$ 150 nm), similar images show these standing wave patterns more obviously [12].

By comparing the near-field images below and above the metal surface (figures 4(a), (c) and (b), (d), respectively) as well as the cross-cuts (figures 4(e), (f)), one can realize a strong difference in the change in near-field intensity over the gold–air interface. This is related to the fundamental difference in the polarizations of the corresponding field components. In regions where the electric field is mostly parallel to the

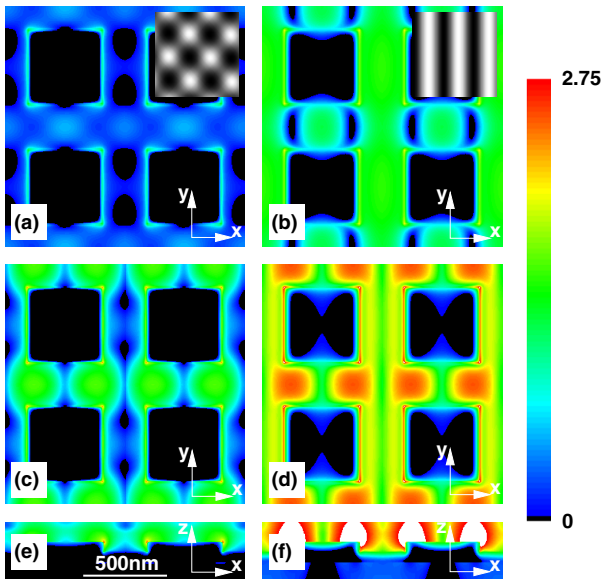

Figure 4. Calculated optical near-field intensities for the [1 1] (a), (c) and (e) and [1 0] (b), (d) and (f) resonance for the array with $\Lambda_x = 760$ nm, $\Lambda_y = 750$ nm and $d_x = d_y = 465$ nm, in cross-cuts parallel to the substrate, 5 nm below ((a), (b)) and above ((c), (d)) the film surface and in cross-cuts perpendicular to the substrate through the centre of the particles ((e), (f)). Plotted quantity: $\log(\frac{|E(\mathbf{r},\lambda)|^2}{|E(\lambda)|^2})$, where $E(\mathbf{r}, \lambda)$ is the electric field amplitude of the array and $E(\lambda)$ is the electric field amplitude in the top layer of a flat surface. The excitation is polarized parallel to x. The insets in (a) and (b) show the interference pattern of similar SPP waves on a flat interface.

(This figure is in colour only in the electronic version)

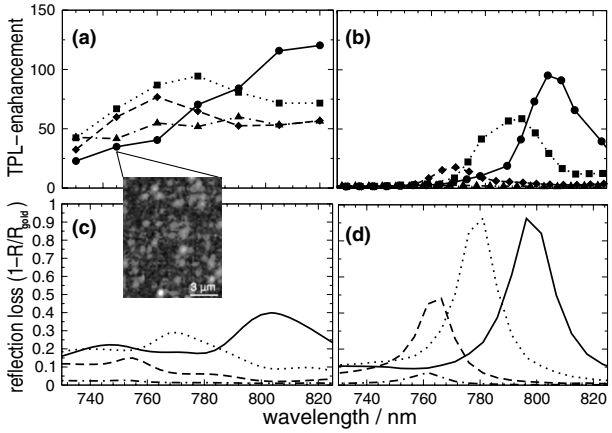

Figure 5. Experimental (a) and simulated (b) TPL enhancement; (c) experimental and (d) simulated reflection loss spectra for the same spectral range for arrays with $\Lambda_x = 760$ nm, $\Lambda_y = 750$ nm and $d_x = d_y = 160$ nm (dash-dotted lines), $d_x = d_y = 265$ nm (dashed lines), $d_x = d_y = 364$ nm (dotted lines), and $d_x = d_y = 465$ nm (solid lines). Inset: TPL microscopy image of the latter sample recorded off-resonance at 745 nm.

gold–air interface, the fields are continuous across the metal–air interface, but close to the particle edges (see especially figure 4(e)) the electric field also has a considerable component vertical to the gold–air interface and is therefore larger in air by the ratio of the dielectric constants of air to gold (i.e. ∼24, leading to a maximum intensity jump of $24^2 = 576$ in the case where the electric field is purely perpendicular to the interface). For the current case, we can infer a maximum area-averaged (over the particle array unit cell) intensity enhancement of ∼2000 just outside the particles (in air), compared to ∼100 just below the gold–air interface inside the gold, as probed by TPL microscopy (see below). This detail highlights the complementary nature of TPL signals investigated here versus other methods which probe the optical near-fields (e.g. surface enhanced Raman scattering (SERS) or any type of optical near-field microscopy) just outside the metal.

Considering the near-field intensity distributions in figure 4, a question arises about the effective surface zone responsible for the strong near-field intensity enhancement and the measured TPL enhancements. A closer analysis shows that, in any case of large near-field enhancements and TPL signals, the strong fields are mostly localized to the particle edges, even if the delocalized SPP fields play a major role in the corresponding resonance. However, the SPP resonance excitation indirectly gives rise to the near-field and TPL enhancements, since the SPPs provide additional 'illumination' of the particles, thereby contributing to the formation of strong fields around the particle edges.

4.1. Two-photon luminescence

To appraise the physical relevance of the FDTD-simulated near-fields, it is vital to find a way to also measure them. In this work we decided to use the TPL of the gold itself, i.e. a third-order nonlinear process [17]. Compared to other near-field measurements (e.g. with the help of Raman-active molecules, fluorescing molecules or dielectric or metallic near-field probes for scanning near-field optical microscopy, SNOM) this has the advantage that no additional ambiguities concerning the probe positions (molecules) or the influence of the changed dielectric environment (SNOM probes) are added. To avoid the complicated calculation and measurement of absolute TPL intensities, we only evaluate the relative TPL enhancement, i.e. the area-averaged TPL signal from the array in relation to the average TPL signal from a smooth gold surface, which by appropriate normalization [12] is proportional to the area-averaged (over the particle array unit cell) near-field intensity enhancement.

To simulate the TPL or near-field intensity enhancements as measured by our setup, we assume that the TPL is proportional to the square of the optical near-field intensity in the *top layer* of our gold surface. By calculating near-field maps similar to figure 4 and integrating the near-field intensities in the top gold layer over the unit cell at different wavelength, we can simulate the area-averaged TPL enhancements expected for such samples and compare them to experimental values [12]. Figure 5 depicts the measured TPL spectra (part (a)) together with the simulation results (part (b)) for arrays with the [1 0] SPP resonance in the spectral region accessible to our TPL setup, i.e. $\Lambda_x = 750$ nm, $\Lambda_y = 760$ nm and varying particle dimensions.

It is clearly seen from the experimental results that the array with $d_x = d_y = 465$ nm produces the highest average TPL enhancements of ∼120, whereas the arrays with smaller particle sizes result in lower enhancements, with their peak positions moving towards shorter wavelengths. These features agree well with the trends observed in the enhancement

spectra calculated using the FDTD approach. One can further observe that, except for the smallest particle size, the measured maximum TPL enhancements actually agree with the calculation results within a factor of two. However, the experimental TPL peaks are broader and less pronounced compared to the calculated TPL peaks, a difference which is consistent with the tendency observed when comparing measured and simulated reflection spectra, figures 5(c) and (d).

5. Comparison of simulations and experiments

Despite the good qualitative agreement between simulations and experiments, there are also significant deviations. The observed differences between the experimental and simulated reflection spectra (figures 3, 5(c), (d)) and the TPL enhancement spectra (figures 5(a), (b)) may originate from several reasons: (i) experimental variations in particle size and array period; (ii) the finite numerical aperture of the spectrometer setup (not considered in the simulations); (iii) the TPL excitation and detection geometry; (iv) deviations of the dielectric function of gold between the actual sample and the Drude–Lorentz fit used for FDTD simulations, including non-locality effects and spatial variations; (v) surface roughness (not considered in the simulations); and (vi) influences of the FDTD boundary conditions and the finite array size. A detailed consideration of the different possibilities leads to the following estimations of the different contributions.

(i) Experimental variations in the particle size and array period: due to the fabrication tolerances, the geometrical parameters of our samples may vary on the order of ∼10 nm, i.e. by 2%. This causes small phase mismatches in the case of grating coupling to SPP and, related to that, a weakening and broadening of the corresponding resonances. The changes in the peak position caused by such variations are, at maximum, ∼15 nm and can therefore partly account for the experimentally observed broader peaks. However, for the localized resonance at ∼520 nm, these variations are insufficient to explain the larger experimentally observed peak width in the reflection-loss spectra, since this peak is basically independent of variations in the particle shape in this range [12].

(ii) The finite numerical aperture of the spectrometer setup: the finite numerical aperture of the spectrometer setup leads to an angular spread of the incident light. At inclined incidence of a plane wave, the reflection-loss peaks caused by grating coupling to SPP modes split into a blue-shifted contribution and a red-shifted contribution. For an angular spread corresponding to NA = 0.075, as in our experiments, this would cause a peak broadening of, at maximum, ∼120 nm at a light wavelength of ∼800 nm, depending on the effective NA of the illumination path (angular intensity distribution).

(iii) The TPL excitation and detection geometry: the observed difference with the simulations might partly be due to the fact that the TPL measurements use a tightly focused beam with a (correspondingly) wide angular spectrum and a small spot-size of only ∼1 μm. This can result in both a broadening of the peaks and an increase in the background by facilitating SPP excitation at about any wavelength in our wavelength range (contrary to what one has in simulations). Moreover, the TPL radiation originating from gold areas with strong field enhancements has unknown angular distribution and interacts with the scattering system (i.e. the particle array), so that the detected TPL is in fact also subject to all scattering phenomena (e.g. scattering at surface roughness and coupling to SPP resonances) considered above for the illuminating radiation. However, for coupling to SPP modes we do not expect any relevant influence of the grating, since the propagation length of SPPs at the spectral range below 550 nm is too low to lead to any grating effects for the array periods considered here [18]. Additionally, the experimental results are affected by the circumstance that the rather weak TPL signals exhibit considerable uncertainties, especially for longer wavelengths, due to inaccuracy in the focus adjustment, possible gradual damage of the sample, etc.

(iv) Deviations of the dielectric function of gold between the actual sample and the Drude–Lorentz fit used for FDTD simulations: for the FDTD simulations, the frequency-dependent data of the experimentally measured dielectric function of gold [16] are fitted by a Drude–Lorentz behaviour [19, 20]. This leads to a very good approximation at larger wavelength, but increasing mismatch with decreasing wavelength in the range below 500 nm. This mismatch can account for deviations between simulated and measured reflection spectra at shorter wavelength and could be reduced by, for example, adding a second Drude term to the fit. Additionally, the effective dielectric function of the gold film and gold particles could deviate from the literature values (e.g. due to surface morphology; see below).

(v) Surface roughness: through detailed analysis of the SEM image of the arrays (figure 2(b)), one can realize a structural difference between the polycrystalline gold film and particle surfaces, i.e. there are smaller grains (∼20 nm) in diameter and ripples on the particles compared to larger crystallites in the size range ∼50–500 nm on the film outside the particles. This qualitative difference in the gold nanostructure comes from the surface processing when fabricating the particles and might cause changes in the effective dielectric function, especially an increase in the imaginary part due to enhanced surface scattering. This contributes to the less pronounced, weaker peaks in the experimental reflection and TPL spectra. Additionally, the surface corrugations lead to additional localized resonances, which are most visible in TPL images recorded off-resonance (the inset of figure 5) by the randomly distributed bright spots, whose positions depend on the excitation wavelength. On average over a larger area, these resonances do not lead to spectrally confined features, but are responsible for the offset in the measured TPL compared to simulations and for the fact that the TPL enhancement levels measured far from the resonances (especially for the $d_x = d_y = 160$ nm particle array) do not approach unity.

(vi) Influences of the boundary conditions: on the vertical walls of the unit cells, the simulations consider strictly

periodic boundary conditions, i.e. infinite arrays, but the experimentally investigated arrays are certainly finite ($100 \times 100\ \mu m^2$). However, since the propagation length, and therefore the interaction distance between the particles ($\sim$20 μm at 800 nm wavelength), is much smaller than the array's size, we do not expect relevant modifications of the results. On the bottom and top boundaries of the volume considered in the FDTD simulations, absorbing boundary conditions realized by a combination of a 'Uniaxial Perfectly Matched Layer' (PML) [21] and a 'Concurrent Complementary Operator Method' layer (CCOM) at a distance of $\sim$0.6 μm above and below the gold film are applied [15]. This is to better absorb the energy flowing at grazing incidence, which is of special importance in the system that is considered, as small SPP peaks in reflection have to be resolved and small errors in the reflection of grazing modes due to an unwanted lack of absorption by the absorbing layers could be attributed spuriously to SPP resonances. Since this combination of PML and CCOM is carefully chosen and tested for the simulations, we also do not expect artefacts in the spectra or near-fields arising from these boundaries.

The only difference, which cannot be explained directly by the above contribution, is the much weaker appearance of the reflection-loss peak related to grazing light modes (peak 'D', figure 3). In other experiments [22] similar peaks are only observed if they overlap with another resonance of the system. Therefore, its strong appearance in our experiments is also related to its overlap with the SPP [1 0] resonance, so that its weakness in the simulations stems from the narrower width of the SPP reflection dips and the correspondingly smaller overlap.

6. Conclusion

In conclusion, we have been able to clarify the nature of the different modes present in regular arrays of gold nanoparticles on gold film measured by reflection spectroscopy and TPL microscopy. By a careful comparison of experimental results versus FDTD simulations, we could identify the parameters responsible for the observed differences. To overcome these differences between simulations and experiment, an improved experimental control of surface structure and crystallinity of the gold film and particles and better knowledge of the gold dielectric function are crucial. For the simulations, the possibility of also including surface roughness would lead to a substantial improvement. However, the generally reasonably good agreement between simulations and experiment can be interpreted in a way such that macroscopic Maxwell equations, as solved by the FDTD code, are suitable for a detailed description of similar systems.

Acknowledgments

The authors acknowledge support from the European Network of Excellence, Plasmo-Nano-Devices (FP6-2002-IST-1-507879), the STREP 'Surface Plasmon Photonics' (FP6-NMP4-CT-2003-505699), the NABIIT project (contract no. 2106-05-033 from the Danish Research Agency) and the Spanish Ministery of Education and Science (grant MAT2005-06608-C02).

References

[1] Moskovits M 1985 *Rev. Mod. Phys.* **57** 783
[2] Nie S and Emroy S R 1997 *Science* **275** 1102
[3] Schuck P J, Fromm D P, Sundaramurthy A, Kino G S and Moerner W E 2005 *Phys. Rev. Lett.* **94** 017402
[4] Beversluis M R, Bouhelier A and Novotny L 2003 *Phys. Rev.* B **68** 115433
[5] Lakowicz J R 2001 *Anal. Biochem.* **298** 1–24
[6] Lakowicz J R *et al* 2002 *Anal. Biochem.* **301** 261–77
[7] Kreibig U and Vollmer M 1995 *Optical Properties of Metal Clusters* (*Springer Series in Materials Science No 25*) (Berlin: Springer)
[8] Beermann J and Bozhevolnyi S I 2005 *Phys. Status Solidi* c **2** 3983
[9] Beermann J, Bozhevolnyi S I, Pedersen K and Fage-Pedersen J 2003 *Opt. Commun.* **221** 295
[10] McCord M A and Rooks M J 1997 *Handbook of Microlithography, Micromachining and Microfabrication* vol 1 (Bellingham, WA: SPIE and the Institute of Electrical Engineers)
[11] Félidj N, Aubard J, Lévi G, Krenn J R, Schider G, Leitner A and Aussenegg F R 2002 *Phys. Rev.* B **66** 245407
[12] Hohenau A, Krenn J R, Beermann J, Bozhevolnyi S I, Rodrigo S G, Martin-Moreno L and Garcia-Vidal F 2007 *Phys. Rev.* B **75** 085104
[13] Lévêque G and Martin O J F 2006 *Opt. Lett.* **31** 2750
[14] Cesario J, Quidant R, Bandenes G and Enoch S 2005 *Opt. Lett.* **30** 3404
[15] Hohenau A, Krenn J R, Beermann J, Bozhevolnyi S I, Rodrigo S G, Martin-Moreno L and Garcia-Vidal F 2006 *Phys. Rev.* B **73** 155404
[16] Johnson P B and Christy R W 1972 *Phys. Rev.* B **6** 4370
[17] Shen Y R 1984 *The Principles of Nonlinear Optics* (New York: Wiley)
[18] Dionne J, Sweatlock L, Polman A and Atwater H 2005 *Phys. Rev.* B **72** 075405
[19] Taflove A and Hagness S C 2000 *Computational Electrodynamics. The Finite-Difference Time-Domain Method* (Boston, MA: Artech House)
[20] Luebbers R J 1992 FDTD for Nth-order dispersive media *IEEE Trans. Antennas Propag.* **40** 1297–301
[21] Zhao L and Cangellaris A C 1996 GT-PML: generalized theory of perfectly matched layers and its application to the reflectionless truncation of finite-difference time-domain grids *IEEE Trans. Microw. Theory Tech.* **44** 2555–63
[22] Félidj N, Laurent G, Aubard J, Lévi G, Hohenau A, Krenn J R, Leitner A and Aussenegg F R 2005 *J. Chem. Phys.* **123** 221103